An Adaptive Symbol Decomposition With Serial Transmission for O-OFDM-Based VLC System

Kejun Jia, Boran Yang, Minghua Cao, Ying Lin, Suoping Li, *Member, IEEE*, and Li Hao, *Member, IEEE*

***Abstract*— In this letter, an adaptive symbol decomposition with serial transmission (ASDST) scheme is proposed to reduce the effect of non-linear clipping noise for optical orthogonal frequency division multiplexing (O-OFDM) system in visible light communication. The transmitted O-OFDM symbol is adaptively decomposed by amplitude clipping and the decomposed symbols are fed into single light emitting diode (LED) by using serial framing. Adaptive symbol decomposition is the process of repeating the amplitude clipping according to each decomposition symbol amplitude and clipping levels. The simulation results show that the ASDST scheme offers improved transmission performance compared with conventional iterative signal clipping (ISC) scheme, since it eliminates all-zero symbols and transmits the same information with fewer decomposition symbols.**

***Index Terms*— Visible light communication, ASDST, O-OFDM, ISC, clipping noise.**

I. Introduction

With the rapid popularization of mobile Internet and intelligent facilities, the spectrum resources of radio frequency (RF) wireless communication are extremely exploited. Recently, visible light communication (VLC) has gained great attention because of its unregulated bandwidth at the optical frequency for wireless communications [1]. The communication signals can be encoded in the visible light spectrum range around $400-700$ nm by using light emitting diode (LED) normally used for illumination [2].

Optical orthogonal frequency division multiplexing (O-OFDM) has been widely applied in VLC systems due to its abilities in resisting the inter symbol interference. To transmit real-valued non-negative signals in intensity modulation and direct detection (IM/DD) based VLC systems, asymmetric clipping O-OFDM (ACO-OFDM) and DC-biased O-OFDM (DCO-OFDM) have been employed. However, the inverse fast Fourier transform (IFFT) operation in the time domain leads to high peak-to-average power ratio (PAPR) for O-OFDM [3]. This high PAPR causes severe non-linear distortion because of the LED non-linearities in VLC systems [4].

There are two methods to mitigate LED non-linear distortion. One is to compensate the non-linear transfer characteristics of LED by pre-distortion or post-distortion. The pre-distortion technique requires additional feedback physical circuits at the transmitter, which degrades the system cost efficiency [5]. Computational complexity and processing delay are the major drawbacks of post-distortion technique [6]. Another method is to suppress LED non-linear clipping distortion by reducing the PAPR of O-OFDM symbol. Iterative signal clipping (ISC) [7] scheme is based on repeated decomposition of high PAPR O-OFDM symbol and transmission from multiple LEDs transmitter. The received symbols from the different LEDs add coherently at the receiver. However, the ISC scheme requires multiple LEDs to emit light simultaneously, which is complicated in synchronization and hardware applications. Symbol decomposition times of the ISC scheme are fixed, the decomposed symbols contain multiple all-zero symbols without loading information, which leads to the decrease of bit error rate (BER) performance. In addition, the channel path gains from each LED to the receiver photodiode (PD) are different and the BER performance deteriorates with channel gain difference.

In this letter, we propose an adaptive symbol decomposition with serial transmission (ASDST) scheme to reduce the non-linear clipping distortion for O-OFDM system. The O-OFDM symbol is adaptively decomposed by amplitude clipping and the serially framed decomposition symbols are fed into single LED. Clipping is adaptively repeated until O-OFDM symbol is completely decomposed or the maximum symbol decomposition times are attained. Compared with the ISC scheme, the main contributions of this letter are summarized in many aspects: i) the decomposed symbols are entered into single LED in serial framing to avoid channel gain difference; ii) the proposed adaptive symbol decomposition mechanism eliminates all-zero symbols, which enhances BER performance for O-OFDM system; iii) the ASDST scheme adopts an unconstrained single LED, which facilitates simple hardware implementation and convenient deployment.

II. System Model

Fig. 1 shows the block diagram of the ASDST scheme for O-OFDM system. The binary data bits are modulated employing Gray coded M-ary quadrature amplitude modulation (QAM) and the subcarriers $\boldsymbol{X}$ are symmetrically expanded with complex conjugate to obtain $\boldsymbol{X}_{\mathrm{mapping}}$ [4].

In order to investigate the connection between O-OFDM symbol variance σ_0^2 and symbol decomposition times,

Manuscript received October 1, 2020; revised October 29, 2020; accepted November 17, 2020. Date of publication November 27, 2020; date of current version March 10, 2021. This work was supported by NSFC projects (61461026 and 61875080). The associate editor coordinating the review of this letter and approving it for publication was C. Gong. *(Corresponding author: Kejun Jia.)*

Kejun Jia, Boran Yang, Minghua Cao, and Ying Lin are with the School of Computer and Communication, Lanzhou University of Technology, Lanzhou 730050, China (e-mail: kjjia@lut.edu.cn; 327467716@qq.com; caominghua@lut.edu.cn; bhfrlin@163.com).

Suoping Li is with the School of Science, Lanzhou University of Technology, Lanzhou 730050, China (e-mail: lsuop@163.com).

Li Hao is with the School of Information Science and Technology, Southwest Jiaotong University, Chengdu 610031, China (e-mail: lhao@home.swjtu.edu.cn).

Digital Object Identifier 10.1109/LCOMM.2020.3041122

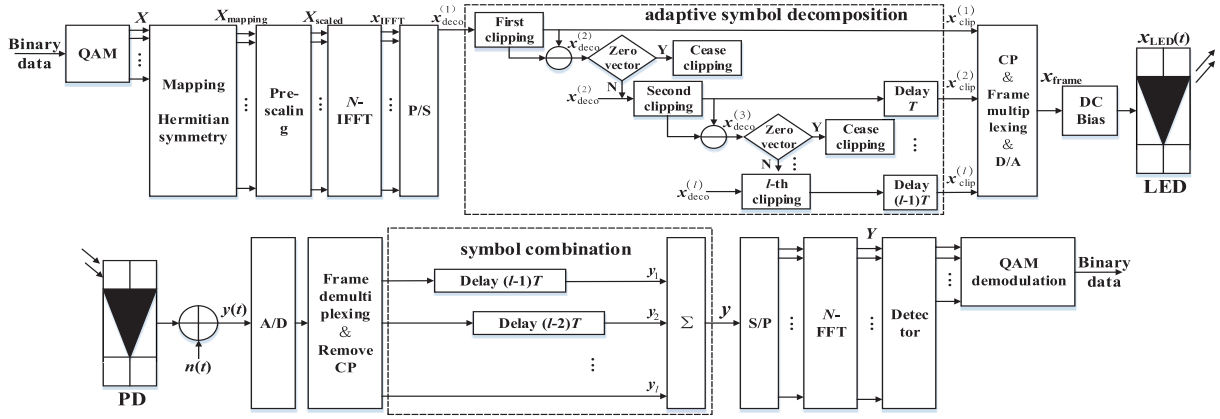

Fig. 1. Block diagram of the ASDST scheme for O-OFDM system.

the pre-scale factor α is introduced to regulate σ_0^2. Pre-scaling of the mapping vector is expressed as $\boldsymbol{X}_{\text{scaled}} = \alpha \boldsymbol{X}_{\text{mapping}}$. The transmitted time domain O-OFDM symbol $\boldsymbol{x}_{\text{IFFT}}$ is obtained by IFFT operation of $\boldsymbol{X}_{\text{scaled}}$ as $\boldsymbol{x}_{\text{IFFT}} = \alpha \boldsymbol{F}^{\text{H}} \boldsymbol{X}_{\text{mapping}}$, where $(\cdot)^{\text{H}}$ denotes the complex conjugate transpose, $\boldsymbol{F}$ is the unitary discrete Fourier transform matrix. The pre-scale factor can be expressed as $\alpha = \sqrt{(N-1)/\sum_{n=0}^{N-1} |\, X_{\text{mapping}}(n)\,|^2}$, where N is the number of subcarriers [8].

Note that $\text{E}[\alpha^2]$ can be simplified to $\text{E}[\alpha^2] = \sigma_0^2/\zeta$ for large N. Here, ζ is the bandwidth efficiency factor, i.e., $\zeta = (N-2)/N$ in DCO-OFDM and $\zeta = 1/2$ in ACO-OFDM. Therefore, the average electrical symbol power of data subcarriers can be expressed as $P_{\text{s,elec}} = \sigma_0^2/\zeta$.

Assuming that the linear dynamic range of LED is $V_{\min}$ to $V_{\max}$. In order to guarantee the bipolar O-OFDM symbol to be non-negative, the LED should be biased by B_{DC} and the bipolar O-OFDM symbol is clipped between $\varepsilon_{\text{bottom}}$ and ε_{top}. The DC bias is set in the middle between $V_{\min}$ and $V_{\max}$ to mitigate non-linear clipping distortion. In ACO-OFDM, the clipping levels at the bottom and top are $\varepsilon_{\text{bottom}} = \max(V_{\min} - B_{\text{DC}}, 0)$ and $\varepsilon_{\text{top}} = V_{\max} - B_{\text{DC}}$ [8]. In DCO-OFDM, the clipping levels at the bottom and top are $\varepsilon_{\text{bottom}} = V_{\min} - B_{\text{DC}}$ and $\varepsilon_{\text{top}} = V_{\max} - B_{\text{DC}}$ [8].

Symbol decomposition is defined as the repeated clipping of large-amplitude O-OFDM symbol into multiple small-amplitude symbols within the dynamic range of LED. The original O-OFDM symbol is restored by summing the decomposed symbols at the receiver. It is possible that $\boldsymbol{x}_{\text{IFFT}}$ contains large-amplitude variables due to its Gaussian distribution. In order to avoid the continuous reduction of information rate and spectral efficiency due to excessive times of symbol decompositions, the maximum symbol decomposition times L are pre-defined.

The following describes the adaptive symbol decomposition in detail. $\boldsymbol{x}_{\text{IFFT}}$ is parallel-to-serial converted into $\boldsymbol{x}_{\text{deco}}^{(1)}$. Adaptive symbol decomposition is the process of repeating the amplitude clipping according to O-OFDM symbol amplitude, clipping levels and L. The symbol $\boldsymbol{x}_{\text{deco}}^{(1)}$ is clipped for the first time and the clipped output $\boldsymbol{x}_{\text{clip}}^{(1)}$ is taken as the result of the first symbol decomposition. Then $\boldsymbol{x}_{\text{clip}}^{(1)}$ is subtracted from $\boldsymbol{x}_{\text{deco}}^{(1)}$ and $\boldsymbol{x}_{\text{deco}}^{(2)} = \boldsymbol{x}_{\text{deco}}^{(1)} - \boldsymbol{x}_{\text{clip}}^{(1)}$ is taken as the decision symbol of whether the second symbol decomposition is required. The symbol decomposition is ceased when $\boldsymbol{x}_{\text{deco}}^{(2)} = \boldsymbol{0}$ or $\boldsymbol{x}_{\text{deco}}^{(2)}$ is used as input for the second symbol decomposition when $\boldsymbol{x}_{\text{deco}}^{(2)} \neq \boldsymbol{0}$. $\boldsymbol{x}_{\text{deco}}^{(2)}$ is clipped for the second time and the clipped output is delayed by one O-OFDM symbol period T to obtain the result $\boldsymbol{x}_{\text{clip}}^{(2)}$ of the second symbol decomposition. Then $\boldsymbol{x}_{\text{clip}}^{(2)}$ is subtracted from $\boldsymbol{x}_{\text{deco}}^{(2)}$ and $\boldsymbol{x}_{\text{deco}}^{(3)} = \boldsymbol{x}_{\text{deco}}^{(2)} - \boldsymbol{x}_{\text{clip}}^{(2)}$ is taken as the decision symbol of whether the third symbol decomposition is required. The symbol decomposition is ceased when $\boldsymbol{x}_{\text{deco}}^{(3)} = \boldsymbol{0}$ or $\boldsymbol{x}_{\text{deco}}^{(3)}$ is used as input for the third symbol decomposition when $\boldsymbol{x}_{\text{deco}}^{(3)} \neq \boldsymbol{0}$. The process is repeated until each decomposition symbol is within the dynamic range of LED or L are attained. The input of the l-th symbol decomposition is $\boldsymbol{x}_{\text{deco}}^{(l)}$, and the clipped output is delayed by time $(l\text{-}1)T$ to obtain $\boldsymbol{x}_{\text{clip}}^{(l)}$. The l-th clipping is expressed as

$$x_{\text{clip}}^{(l)}(k) = \begin{cases} \varepsilon_{\text{top}}, & x_{\text{deco}}^{(l)}(k) \geq \varepsilon_{\text{top}}, \\ x_{\text{deco}}^{(l)}(k), & \varepsilon_{\text{bottom}} < x_{\text{deco}}^{(l)}(k) < \varepsilon_{\text{top}}, \\ \varepsilon_{\text{bottom}}, & x_{\text{deco}}^{(l)}(k) \leq \varepsilon_{\text{bottom}}, \end{cases} \tag{1}$$

where $1 \leq l \leq L$, $x_{\text{deco}}^{(l)}(k)$ and $x_{\text{clip}}^{(l)}(k)$ represent the k-th variable of $\boldsymbol{x}_{\text{deco}}^{(l)}$ and $\boldsymbol{x}_{\text{clip}}^{(l)}$ for $k = 0, 1, \ldots, N-1$.

Assuming that the adaptive symbol decomposition terminates after l times, $\boldsymbol{x}_{\text{clip}}^{(1)}$, $\boldsymbol{x}_{\text{clip}}^{(2)}$, …, $\boldsymbol{x}_{\text{clip}}^{(l)}$ are the results of symbol decomposition. $\boldsymbol{x}_{\text{deco}}^{(1)}$ is actually a vector, when the amplitudes of all subcarriers forming $\boldsymbol{x}_{\text{deco}}^{(1)}$ are within $[L\varepsilon_{\text{bottom}}, L\varepsilon_{\text{top}}]$, the required times of symbol decompositions are $1 \leq l \leq L$ and $\boldsymbol{x}_{\text{deco}}^{(1)}$ is completely transmitted. However, when the amplitudes of partial subcarriers exceed $[L\varepsilon_{\text{bottom}}, L\varepsilon_{\text{top}}]$, the required times of symbol decompositions attain L and $\boldsymbol{x}_{\text{deco}}^{(1)}$ is partially transmitted, which results in non-linear clipping distortion and can be modeled by means

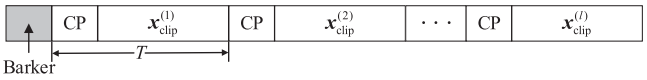

Fig. 2. Frame structure.

of the Bussgang theorem as

$$\boldsymbol{x}_{\text{clip}} = \boldsymbol{x}_{\text{clip}}^{(1)} + \boldsymbol{x}_{\text{clip}}^{(2)} + \cdots + \boldsymbol{x}_{\text{clip}}^{(L)} = \eta \boldsymbol{x}_{\text{IFFT}} + \boldsymbol{n}_{\text{clip}}, \quad (2)$$

where $\boldsymbol{n}_{\text{clip}}$ is the zero-mean non-Gaussian clipping noise, η is the amplitude attenuation factor calculated by $\eta = Q(L\lambda_{\text{bottom}}) - Q(L\lambda_{\text{top}})$, $\lambda_{\text{bottom}} = \varepsilon_{\text{bottom}}/\sigma_0$ and $\lambda_{\text{top}} = \varepsilon_{\text{top}}/\sigma_0$ are the normalized bottom and top clipping level respectively, $Q(\cdot)$ is the complementary cumulative distribution function.

The decomposition symbols with cyclic prefix (CP) are encapsulated into frame in series. Frame synchronization is achieved rapidly using the Barker sequence as the head of the serial frame $\boldsymbol{x}_{\text{frame}}$. Frame structure is shown in Fig. 2.

The frame is digital-to-analog converted and DC biased resulting in $x_{\text{LED}}(t) = x_{\text{frame}}(t) + B_{\text{DC}}$. Regardless of the influence of CP and frame header, when the symbol transmission rate of LED is constant, the bit rate R_{b} of the ASDST scheme is $1/l$ of the ISC scheme, i.e., $R_{\text{b}} = \zeta W \log_2(M)/2l$, where W is the modulation bandwidth of O-OFDM symbol. Therefore, the spectral efficiency of the ASDST scheme can be calculated as $n_{\text{b}} = R_{\text{b}}/W$.

At the receiver, the electrical signal is expressed as $y(t) = \gamma x_{\text{LED}}(t) + n(t)$ [3], where γ is the responsivity of the PD receiver, $n(t)$ is an additive white Gaussian noise (AWGN) with single-sided power spectral density (PSD) of N_0. $y(t)$ is analog-to-digital converted and the frame is identified from the received data using the frame header detector. After removing the frame header, the frame is sampled to restore the decomposition symbols. The decomposed symbols are distinguished by the correlation between each CP and the corresponding O-OFDM symbol [7]. The CP is deleted and all symbols are delayed to obtain time domain synchronized $\boldsymbol{y}_1$, $\boldsymbol{y}_2$, …, $\boldsymbol{y}_l$. Furthermore, the corresponding addition of the decomposed symbols can be expressed as

$$\boldsymbol{y} = \gamma[\boldsymbol{x}_{\text{clip}}^{(1)} + \boldsymbol{x}_{\text{clip}}^{(2)} + \cdots + \boldsymbol{x}_{\text{clip}}^{(l)}] + \gamma l \boldsymbol{B} + \boldsymbol{n}_1 + \boldsymbol{n}_2 + \cdots + \boldsymbol{n}_l, \quad (3)$$

where $\boldsymbol{B} = [B_{\text{DC}}, B_{\text{DC}}, \ldots, B_{\text{DC}}]^{\text{T}}$, $\boldsymbol{n}_l$ is the AWGN on the l-th decomposition symbol with the identical PSD.

$\boldsymbol{y}$ is serial-to-parallel converted and input to an N-point FFT, the output frequency domain signal is expressed as

$$\boldsymbol{Y} = \alpha\gamma\eta \boldsymbol{X}_{\text{mapping}} + \gamma \boldsymbol{N}_{\text{clip}} + \gamma l \hat{\boldsymbol{B}}_{\text{DC}} + l \boldsymbol{N}_{\text{AWGN}}, \quad (4)$$

where $\hat{\boldsymbol{B}}_{\text{DC}} = [\sqrt{N} B_{\text{DC}}, 0, 0, \ldots, 0]^{\text{T}}$, $\boldsymbol{N}_{\text{AWGN}}$ and $\boldsymbol{N}_{\text{clip}}$ are the AWGN and clipping noise in frequency domain respectively. For large FFT size, $\boldsymbol{N}_{\text{clip}}$ is transformed to the zero-mean Gaussian noise with variance for ACO-OFDM and DCO-OFDM as follows

$$\begin{aligned}\sigma_{\text{clip,ACO}}^2 = {} & \frac{P_{\text{s,elec}}}{2}\{\eta(L^2\lambda_{\text{bottom}}^2 + 1) - 2\eta^2 \\ & - L\lambda_{\text{bottom}}\left[\varphi(L\lambda_{\text{bottom}}) - \varphi(L\lambda_{\text{top}})\right] \\ & - \varphi(L\lambda_{\text{top}})(L\lambda_{\text{top}} - L\lambda_{\text{bottom}}) \\ & + Q(L\lambda_{\text{top}})(L\lambda_{\text{top}} - L\lambda_{\text{bottom}})^2\}, \quad (5)\end{aligned}$$

$$\begin{aligned}\sigma_{\text{clip,DCO}}^2 = {} & P_{\text{s,elec}}\{\eta - \eta^2 - \{\varphi(L\lambda_{\text{bottom}}) - \varphi(L\lambda_{\text{top}}) \\ & + L\lambda_{\text{bottom}}[1 - Q(L\lambda_{\text{bottom}})] + L\lambda_{\text{top}}Q(L\lambda_{\text{top}})\}^2 \\ & + L^2\lambda_{\text{bottom}}^2[1 - Q(L\lambda_{\text{bottom}})] + L^2\lambda_{\text{top}}^2 Q(L\lambda_{\text{top}}) \\ & + L\lambda_{\text{bottom}}\varphi(L\lambda_{\text{bottom}}) - L\lambda_{\text{top}}\varphi(L\lambda_{\text{top}})\}, \quad (6)\end{aligned}$$

where $\varphi(u) = 1/\sqrt{2\pi}\exp(-u^2/2)$.

$\boldsymbol{Y}$ is equalized and the data subcarriers are extracted according to the mapping manner of O-OFDM symbol. The BER performance for square M-QAM can be referenced [7], [8]. The electrical signal to noise ratio (SNR) per bit can be expressed as

$$\Psi_{\text{SNR}} = \frac{\alpha^2\eta^2\gamma^2 P_{\text{s,elec}}}{\log_2(M)(\sigma_{\text{clip}}^2 + lWN_0)}. \quad (7)$$

III. Simulation Results

In this section we present the results of the simulation. System parameters are listed in Table I. Under this circumstance, it can be calculated that the power of AWGN as $WN_0 = -10$ dBm, $\varepsilon_{\text{bottom}}$ and ε_{top} are 0 V and 0.8 V for ACO-OFDM respectively, the clipping levels at the bottom and top are -0.1 V and 0.8 V for DCO-OFDM respectively. The fixed symbol decomposition times l_{ISC} of the ISC scheme are taken as 6. Since each O-OFDM symbol decomposition times and AWGN are random variables, Monte Carlo method is adopted to obtain the average symbol decomposition times, average BER, average bit rate, and average error vector magnitude (EVM).

Fig. 3 shows the average symbol decomposition times of ISC and ASDST schemes versus the O-OFDM symbol variance. $l_{\text{ISC}} = 6$ and $L = 6$. It can be observed that the proposed scheme has significantly less times of symbol decompositions than the ISC scheme, especially at low symbol variances. For ACO-OFDM and N=256, when the symbol variances are equal to 21.9, 30, and 34 dBm, the average times of symbol decompositions are 2, 4, and 6 with the ASDST scheme respectively. For large N and at the same bit rate, the symbol decomposition times of ACO-OFDM are approximately half that of DCO-OFDM. It is due to that the data transmitted by the ACO-OFDM only about half of the DCO-OFDM under the same number of subcarriers and modulation order. In addition, the symbol PAPR becomes larger as the number of subcarriers N increases, which leads to more symbol decomposition times.

Fig. 4 shows the BER comparison of ISC and ASDST schemes under the same bit rate. $l_{\text{ISC}} = 6$ and $L = 6$. In the ISC scheme, the BER performance deteriorates as the channel gain difference increases. We assume that the channel transmitting the first decomposition symbol is regarded as the standard channel. For ACO-OFDM and σ_0^2=37.9 dBm, BER

TABLE I
SYSTEM PARAMETER.

Parameter	Symbol	Value
Modulation bandwidth	W	20 MHz
Noise PSD	N_0	$5 \times 10^{-12}\mathrm{A}^2/\mathrm{Hz}$
PD responsivity	γ	1 A/W
LED turn-on voltage	$V_{\min}$	0.1 V
LED maximum permissible voltage	$V_{\max}$	1 V
DC bias	B_{DC}	0.2 V

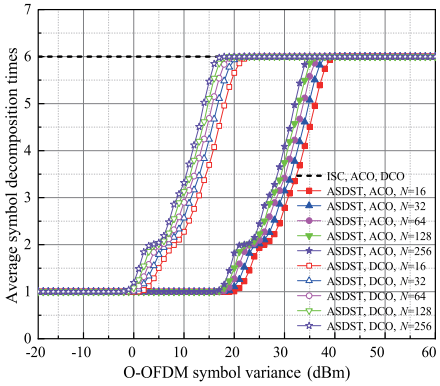

Fig. 3. Average symbol decomposition times of ISC and ASDST schemes using different subcarriers number and modulation sizes of $M = 16$.

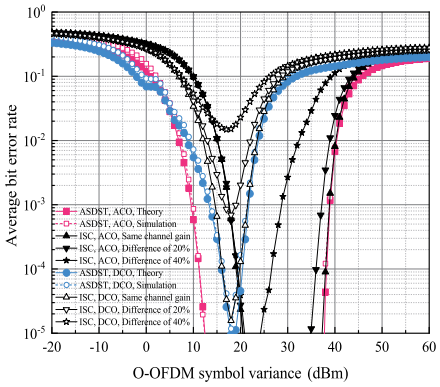

Fig. 4. BER performance comparison between ISC and ASDST schemes using subcarriers number of $N = 256$ and modulation sizes of $M = 16$.

can achieve 10^{-5} when the channel gains are ideally equal. However, when the channel gain differences between other decomposition symbols and the first decomposition symbol are 20% and 40%, BER are approximately 10^{-3} and 10^{-1} respectively. Fortunately, the proposed scheme avoids the channel gain difference by using single LED and achieves a better BER performance.

It is also seen that the performance of theory and simulation results perfectly match in the proposed scheme. At low symbol variances and a BER of 10^{-3}, compared with the ISC scheme, the O-OFDM symbol variance improvements of the proposed ASDST scheme are >7 dBm and ~ 2 dBm for ACO-OFDM and DCO-OFDM respectively. This coincides with the fact that the ASDST scheme eliminates all-zero symbols and reduces the accumulated AWGN at the receiver. At high symbol variances, the average symbol decomposition times of the ASDST scheme attain L. Therefore, the ISC and ASDST

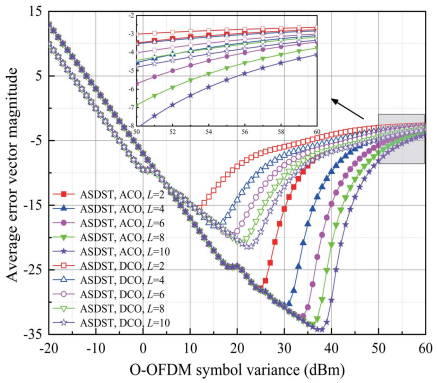

Fig. 5. EVM performance of the ASDST scheme using subcarriers number of $N = 256$ and modulation sizes of $M = 16$ for different L.

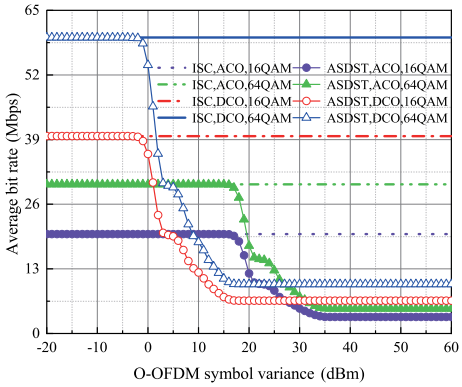

Fig. 6. Average bit rate of ISC and ASDST schemes using subcarriers number of $N = 256$ and modulation sizes of $M = 16$ and 64.

schemes have the same optical transmission power and the same BER performance without considering the channel gain difference.

EVM describes the difference between received and standard constellation points [6]. Fig. 5 shows the EVM performance of the ASDST scheme. At low symbol variances, no clipping noise exists and the performance enhances as the symbol variance increases. However, as the symbol variance increases beyond a certain optimum point, clipping noise appears and the performance decreases with further increase in the symbol variance. Furthermore, at low symbol variances, the average symbol decomposition times are less than L and the performance is independent of L. At high symbol variances, clipping noise is reduced and the performance can be further enhanced by considering more L.

Fig. 6 shows the bit rate comparison of ISC and ASDST schemes under the same LED symbol transmission rate. $l_{\mathrm{ISC}} = 6$ and $L = 6$. At low symbol variances, the ASDST scheme has the same bit rate as the ISC scheme. However, at high symbol variances, the bit rates of the ASDST scheme are reduced with increasing symbol decomposition times. For DCO-OFDM and 16QAM, when the symbol variances are equal to -13 and 13 dBm, the bit rates of the ASDST scheme are 39.7 and 8.96 Mbps respectively. Furthermore, the bit rates of the ASDST scheme are enhanced by increasing the modulation order M.

IV. Conclusion

In this letter, we proposed an ASDST scheme for clipping noise reduction and EVM enhancement in the O-OFDM-based VLC system. The average symbol decomposition times of the proposed ASDST scheme are significantly reduced compared with that of classical ISC scheme, which improved the BER performance at low symbol variances. Compared with the ISC scheme at the same symbol decomposition times, the proposed scheme avoids the BER deterioration caused by multiple asynchronous LEDs and channel gain difference. In addition, the bit rate and spectral efficiency of the proposed scheme are further improved by increasing LED modulation bandwidth and establishing MIMO system.

References

[1] D.-F. Zhang, Y.-J. Zhu, J.-K. Zhang, and Y.-Y. Zhang, "Constellation collaborated OFDM for visible light communication systems," *IEEE Commun. Lett.*, vol. 18, no. 6, pp. 1067–1070, Jun. 2014.

[2] K. M. V. Zwaag, J. L. C. Neves, H. R. O. Rocha, M. E. V. Segatto, and J. A. L. Silva, "Adaptation to the LEDs flicker requirement in visible light communication systems through CE-OFDM signals," *Opt. Commun.*, vol. 441, pp. 14–20, Jun. 2019.

[3] T. Zhang, Y. Zou, J. Sun, and S. Qiao, "Improved companding transform for PAPR reduction in ACO-OFDM-based VLC systems," *IEEE Commun. Lett.*, vol. 22, no. 6, pp. 1180–1183, Jun. 2018.

[4] J.-S. Sheu, B.-J. Li, and J.-K. Lain, "LED non-linearity mitigation techniques for optical OFDM-based visible light communications," *IET Optoelectron.*, vol. 11, no. 6, pp. 259–264, Dec. 2017.

[5] H. Elgala, R. Mesleh, and H. Haas, "Non-linearity effects and predistortion in optical OFDM wireless transmission using LEDs," *Int. J. Ultra Wideband Commun. Syst.*, vol. 1, no. 2, pp. 143–150, Jan. 2009.

[6] H. Qian, S. J. Yao, S. Z. Cai, and T. Zhou, "Adaptive postdistortion for nonlinear LEDs in visible light communications," *IEEE Photon. J.*, vol. 6, no. 4, pp. 1–8, Aug. 2014.

[7] R. Mesleh, H. Elgala, and H. Haas, "LED nonlinearity mitigation techniques in optical wireless OFDM communication systems," *J. Opt. Commun. Netw.*, vol. 4, no. 11, pp. 865–875, Nov. 2012.

[8] S. Dimitrov, S. Sinanovic, and H. Haas, "Clipping noise in OFDM-based optical wireless communication systems," *IEEE Trans. Commun.*, vol. 60, no. 4, pp. 1072–1081, Apr. 2012.